Separated Flow Computations with the k-ε-v^2 Model

P. A. Durbin*

Stanford University, Stanford, California 94035

Turbulent separated flows over a backstep, in a plane diffuser and around a triangular cylinder, are computed with the k-ε-v^2 model. These provide examples of massive separation, of smooth separation, and of unsteady vortex shedding. It is shown that to accurately predict the time-averaged properties of bluff body flow, it is necessary to resolve the coherent vortex shedding. The near-wall treatment of the v^2-f_{22} system of equations is able to cope with both the massive and smooth separations. Good agreement between experiment and prediction is found in all cases.

Introduction

THE primary motivation for developing turbulent transport models is to provide tools for computing nonequilibrium, or complex, turbulent flows. Simple flows can be analyzed using data correlations or algebraic eddy viscosities; but, in more complicated flows, such as a massively separated boundary layer, a more elaborate level of modeling is required. It is widely believed that at least a two-equation transport model is required in such cases. The transport equations determine the evolution of suitable velocity and time scales of the turbulence; for instance, in the standard k-ε model, k is the (squared) velocity scale and k/ε is the time scale. However, the standard k-ε model gives unacceptable results if it is integrated to a solid, no-slip boundary.[1] It was noted by Launder[2] and Durbin[3] that this is because the appropriate velocity scale for turbulent transport toward the wall is $\overline{v^2}$, not k. This, and other, considerations motivated the k-ε-v^2 model,[3,4] which can be used in wall-bounded flows.

Applications to complex geometry require a generalized interpretation of the velocity scale $\overline{v^2}$. The k-ε-$\overline{v^2}$ model originally was developed for attached or mildly separated boundary layers. Rather promising results were obtained in tests of the formulation. In the present paper the model is assessed in strongly separated flows. Doing so requires that $\overline{v^2}$ be regarded simply as a velocity scale that satisfies boundary conditions suitable for the normal component of turbulent intensity; it cannot be regarded as the y component because that would be inappropriate in general geometries that can have surfaces aligned in any direction. This loosened understanding of $\overline{v^2}$ presents no operational difficulties. In steady, two-dimensional flows $\overline{v^2}$ might be regarded as the intensity normal to streamlines, thereby introducing effects of streamline curvature in a natural way; such a formulation will not be pursued here. The equations of the model are presented in the next section.

Governing Equations

The mean flow satisfies the incompressible Navier–Stokes equations with an eddy viscosity:

$$\partial_t U + U \cdot \nabla U = -\nabla P + \nabla \cdot [(v + v_t)\nabla U]$$
$$\nabla \cdot U = 0 \tag{1}$$

The turbulence model uses the standard k-ε equations[1]

$$\partial_t k + U \cdot \nabla k = \mathcal{P} - \varepsilon + \nabla \cdot \left[\left(v + \frac{v_t}{\sigma_k}\right)\nabla k\right]$$

$$\partial_t \varepsilon + U \cdot \nabla \varepsilon = \frac{C_{\varepsilon_1}^z \mathcal{P} - C_{\varepsilon_2}\varepsilon}{T} + \nabla \cdot \left[\left(v + \frac{v_t}{\sigma_\varepsilon}\right)\nabla \varepsilon\right] \tag{2}$$

where the rate of turbulent energy production is

$$\mathcal{P} = v_t(\partial_i U_j + \partial_j U_i)\partial_i U_j \tag{3}$$

On no-slip boundaries

$$k = n \cdot \nabla k = 0$$

where n is the unit vector, normal to the surface. This no-slip condition imposes two boundary conditions on k. No boundary conditions can be imposed on ε (Ref. 4), indeed, the behavior of ε at the wall must be found as part of the solution (see Fig. 7).

The $\overline{v^2}$ transport equation is

$$\partial_t \overline{v^2} + U \cdot \nabla \overline{v^2} = kf_{22} - \overline{v^2}\frac{\varepsilon}{k} + \nabla \cdot \left[\left(v + \frac{v_t}{\sigma_k}\right)\nabla \overline{v^2}\right] \tag{4}$$

The term kf_{22} is the source of $\overline{v^2}$; in the original interpretation of the k-ε-v^2 model[3] it represented redistribution of turbulent intensity from the streamwise component.

Impermeable boundaries cause nonlocal suppression of $\overline{v^2}$. Nonlocality is represented mathematically by an elliptic relaxation equation[4] for f_{22}

$$L^2\nabla^2 f_{22} - f_{22} = (1 - C_1)\frac{[\frac{2}{3} - \overline{v^2}/k]}{T} - C_2\frac{\mathcal{P}}{k} \tag{5}$$

On no-slip boundaries the behavior $\overline{v^2} \to \mathcal{O}(x \cdot n)^4$ as $x \cdot n \to 0$ is enforced by invoking the local solution

$$\overline{v^2} \to \varepsilon(0)f_{22}(0)(x \cdot n)^4/20v^2 \tag{6}$$

to Eq. (4). The differential equations (4) and (5) were formulated so that Eq. (6) amounts to imposing two homogeneous boundary conditions on $\overline{v^2}$ and none on f_{22}; thus, the k-ε and $\overline{v^2}$-f_{22} systems are analogous numerically and were solved with the same subroutines. Boundary condition (6) and Eqs.(4) and (5) make $\overline{v^2}$ behave as the normal component of turbulent intensity near no-slip surfaces.

The length and time scales appearing in the model equations are

$$\ell^2 = \max\left[\frac{k^3}{\varepsilon^2}, C_\eta^2\left(\frac{v^3}{\varepsilon}\right)^{\frac{1}{2}}\right]$$

$$L = C_L\ell \tag{7}$$

$$T = \max\left[\frac{k}{\varepsilon}, 6\left(\frac{v}{\varepsilon}\right)^{\frac{1}{2}}\right]$$

The coefficient of 6 in the expression for T was obtained from direct numerical simulation (DNS) data[3]; although it is a model constant,

results are not sensitive to its value, which has been fixed at 6 once and for all. The eddy viscosity is given by

$$v_t = C_\mu \overline{v^2} T \qquad (8)$$

A model to be used in flows that contain both wall-bounded and free shear layers must incorporate baseline information for each case. The most fundamental information is the shear layer spreading rate. The spreading rate of a mixing layer is higher than that of a boundary layer. At a qualitative level, this reflects a difference between the structure of the large, entrainment eddies in wall-bounded and in free shear layers. There is no obvious way to distinguish such differences in eddy structure within the confines of a simple, single point closure. It might be argued that the energy content in the entrainment eddies is influenced by wall effects and that these depend on the ratio of distance to the wall d to the turbulence scale $k^{\frac{3}{2}}/\varepsilon$.

It is well known that the coefficient $C_{\varepsilon_1}^z$ in the ε-equation (2) controls the shear layer spreading rate. Reference 4, and others, allowed that coefficient to be a function of $\mathcal{P}/\varepsilon$. In some of the more complex flows that we have calculated, the dependence on $\mathcal{P}/\varepsilon$ prevented numerical convergence to a steady solution. However, the constant value of $C_{\varepsilon_1}^z = 1.55$ was found suitable for wall-bounded flows, after the requisite minor revision of other coefficients. Figure 1 [which was actually computed with expression (9)] shows that this value gives the correct evolution of C_f and the correct shape of velocity profiles in a flat plate boundary layer.[5] However, the value of 1.55 gives a too slow spreading rate for plane mixing layers; a value of 1.3 is needed. As a pragmatic device, the function

$$C_{\varepsilon_1}^z = 1.3 + \frac{0.25}{[1 + (d/2\ell)^8]} \qquad (9)$$

of distance d to the closest boundary has been used to interpolate between the values of 1.55 and 1.3 where ℓ is the length scale [(Eq. 7)] of the energetic eddies. The function of d/ℓ was devised such that Eq. (9) gives results that are indistinguishable from $C_{\varepsilon_1}^z = 1.55$ in attached boundary layers and reverts to $C_{\varepsilon_1}^z = 1.3$ far from any surface.

The other constants of the model are

$$C_\mu = 0.19, \qquad C_{\varepsilon_2} = 1.9, \qquad C_1 = 1.4$$
$$C_2 = 0.3, \qquad C_L = 0.3 \qquad C_\eta = 70.0 \qquad (10)$$
$$\sigma_k = 1.0, \qquad \sigma_\varepsilon = 1.3$$

There is leeway to these values. For instance, σ_k was changed from 0.9 in Ref. 4 to 1.0 simply because that is the conventional value. Indeed, it is probable that the model constants can be recalibrated so that the results presented in this paper are reproduced with slightly different values. This is because some of the constants are interconnected; for example, the constants C_L and C_η are related such that increases of C_L can be compensated by decreases of C_η without altering the predictions of the model. This tolerance in the values of constants is common to virtually all turbulence models.

Numerical Method

The computations were done with an extended version of the incompressible Navier–Stokes two-dimensional (INS2D) code of Rogers and Kwak.[6] In this code the incompressible, Reynolds averaged Navier–Stokes equations are solved by an artificial compressibility method. This method has the advantage that the momentum and continuity equations are solved simultaneously, as a coupled system for velocity and pressure. Convective derivatives are approximated by third-order, upwind biased flux-splitting and diffusive terms by central differencing.

The extensions required for the present computations consist of providing subroutines to solve the transport and elliptic relaxation equations of the k-ε-$\overline{v^2}$ model. These equations were solved two at a time, as coupled k-ε and $\overline{v^2}$-f_{22} systems. That makes the finite-difference equations sufficiently implicit to permit large pseudo-time steps in steady-state calculations, without numerical instability. The coupling between pairs of equations is dictated primarily by the no-slip boundary condition. For instance, no slip requires that
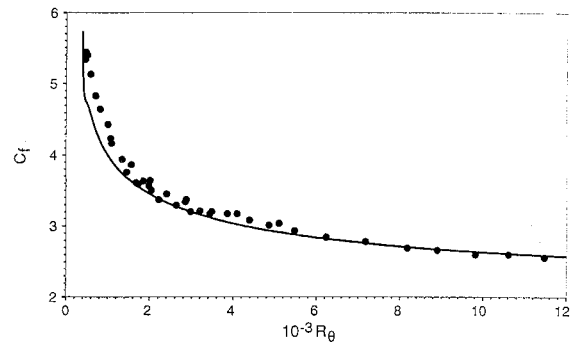

Fig. 1a   Friction coefficient in a zero pressure gradient boundary layer, compared to data from Ref. 5, cases 1400 and 3000.
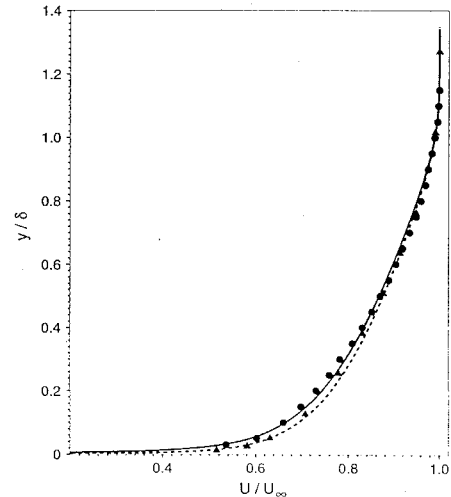

Fig. 1b   Mean velocity profiles at R_θ = 3200 (———, ●) and 10,600 (- - -, ▲) in a zero pressure gradient boundary layer, compared to data from Ref. 5.

two boundary conditions be applied to k and none to ε; this provides the correct number of boundary conditions on the k-ε system.

The intermediate variable f_{22} is the solution to the elliptic relaxation Eq. (5). It should be emphasized that this is not a Poisson equation and does not require any special numerical treatment. If the coefficients in the elliptic relaxation operator were constant, then it would become a forced, modified Helmholtz equation. The Green's function of the modified Helmholtz equation has an exponential decay, so nonlocal influences are confined to the scale of the turbulence; this contrasts to the algebraic decay of the Green's function of the Poisson equation, which gives rise to nonlocal influences on the overall geometric scale. Another virtue of Eq. (5) is that it introduces wall effects via a linear differential equation.

Both the two-dimensional mean flow and the turbulence model equations were written in semi-implicit, Δ form. The implicit matrices were inverted by block tridiagonal, alternating direction implicit (ADI) line relaxation. The blocks are 3×3 for the two-dimensional mean flow and 2×2 for each system of the turbulence equations.

For steady-state computations the time step acts as a relaxation parameter. In the Δ form of the finite-difference equations, the residuals appear on the right-hand side, and the iterations amount to relaxing these residuals. Rather large time steps were possible in all of the computations reported herein; convergence was obtained in the order of 150–200 iterations (the convergence criteria were that a test value became constant to four decimal points; that the maximum divergence of the mean flow was of order 10^{-4}, or less; and that the maximum residual was of order 10^{-6}, or less). The convergence of the present turbulence model seems to be rather robust: the initial guess consisted of setting $k = 4 \times 10^{-4}$, $\overline{v^2} = 2k/3$, $\varepsilon = 6 \times 10^{-6}$, and $f_{22} = 0$ everywhere except on boundaries, where k and $\overline{v^2}$ were set to 0. These arbitrary initial fields evolved quickly to reasonable distributions during the iterations. The normalization here,

and throughout this paper, is on a reference mean velocity and a geometrical length scale.

For the time-accurate computations, each time step of the mean flow was iterated to obtain an incompressible solution. Application of the artificial compressibility method to unsteady flow is described in Rogers et al.[7] Each time step required about 20 subiterations; this reduced the divergence to the order of 10^{-2}, which is the marginal requirement suggested by Rogers et al.[7] for time-accurate computations. The time derivatives in the mean flow equations were approximated by second-order, time-lagged differences; however, to save computer storage and computation time, first-order, semi-implicit differencing was used to integrate the turbulence model. Although the formal accuracy of the time integration is first order, our experience suggests that the lower order differencing of the turbulence transport equations does not substantially reduce the second-order accuracy of the mean flow solution. This is probably because the turbulence affects the mean flow only via an eddy viscosity. The time-accurate, bluff-body calculations that are reported herein required about two orders of magnitude more computation than corresponding steady-state calculation of the same geometry. However, as will be shown, steady-state calculations are unacceptable for a bluff-body flow that contains deterministic vortex shedding.

In addition to the bluff-body flow, computations will be presented of flow over a backstep and in a separated diffuser. A 120 × 120, nonuniform grid was used for the backstep computations. Ko[8] performed a grid refinement study with a model that is analogous to that used herein and found this to be adequate resolution. The diffuser computation used a 124 × 65 grid provided by H. Kaltenbach (of CTR) who generated the grid for large eddy simulation. He also did extensive grid refinement tests. We have not repeated these tests because the requirements of moment closure modeling are less stringent than those of large eddy simulation. The bluff body flow computation used a 141 × 101 grid. Computations on coarser meshes will also be presented to show that this provides adequate resolution.

Results

Flow over Backward Facing Steps

The backstep flow configurations studied experimentally by Jovic and Driver[9] (JD) and by Driver and Seegmiller[10] (DS) were computed with the k-ε-$\overline{v^2}$ model. The JD experiment had a step height Reynolds number of 5,000, an inlet momentum thickness Reynolds number of 600, an expansion ratio of 1.2, and was done in a symmetric channel. DS had a step height Reynolds number of 37,500, an inlet momentum thickness Reynolds number of 5,000, an expansion ratio of 1.125, and a plane wall opposite the step. The inlet profiles for all of the dependent variables were obtained by solving the model at the appropriate momentum thickness Reynolds number with a boundary-layer code. In the figures all velocities are non-dimensionalized by the inlet freestream velocity, and all lengths are scaled on the step height.

Computed and experimental skin friction coefficients on the wall downstream of the step are compared in Fig. 2. The computed reattachment point at $x = 6.2$ step heights is in agreement with the data. The relatively large negative skin friction in the JD experiment is due to the low Reynolds number.[11] The model correctly shows this sensitivity to Reynolds number. The most noticeable discrepancy between the model and the experimental data is in the extent of the small region of positive C_f near $x = 0$. The positive C_f is due to a secondary eddy that sits in the corner at the base of the step, inside the main recirculation region. The size of this secondary eddy is underpredicted, so that the negative dip of the computed skin friction starts too close to the bottom of the step. Overall, the agreement with experiment is better than has been found using the standard k-ε model with wall functions[10]; numerous independent computations have shown that model to underpredict the reattachment length.[12]

Figures 3 and 4 show profiles of the U component of velocity. These profiles are plotted in the form $10U + x$ to display their evolution down the duct. The agreement between model and experiment in the JD case is quite good. In the DS case the agreement is good for $x < 8$ but the model solution for the boundary layer downstream of reattachment recovers more slowly than the data. This
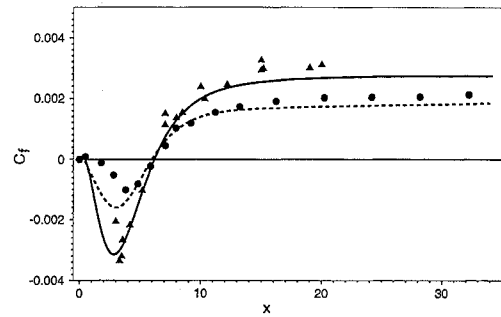

Fig. 2 Skin friction coefficient on wall downstream of the backstep compared to experiments of Jovic and Driver (——, ▲) and Driver and Seegmiller (– – –, ●).
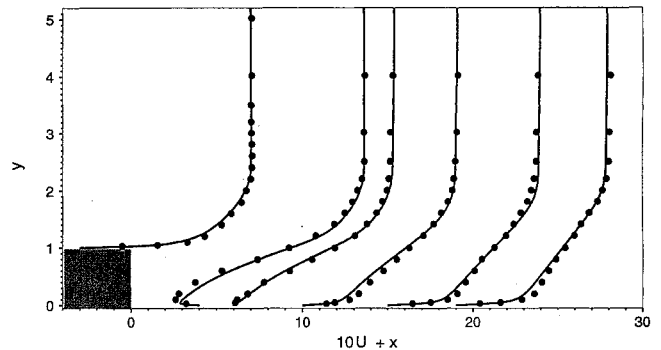

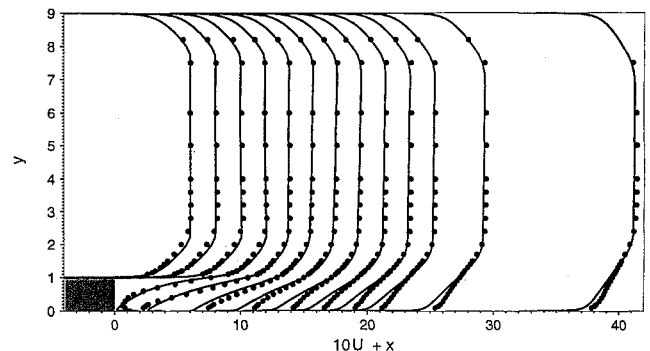Fig. 3 Mean velocity profiles for the Jovic and Driver experiment.

Fig. 4 Mean velocity profiles for the Driver and Seegmiller experiment.

slow recovery downstream of reattachment is a universal problem of turbulence models, shown by Reynolds stress[8] as well as k-ε models.

The focus in the present paper is on properties of the mean flow. Nevertheless, profiles of turbulent kinetic energy for the JD and DS experiments are presented in Figs. 5 and 6. They have been plotted as $100k + x$. The $\overline{w^2}$ component was not measured in the experiments, so the usual approximation $k \approx 3/4(\overline{u^2} + \overline{v^2})$ was used. The k-ε-$\overline{v^2}$ predictions of the JD experiment are very good. For the DS experiment, the predicted turbulent intensity is bit high in the separated region but, generally, is in favorable agreement with the data.

The model variable $\overline{v^2}$ cannot be compared to data on the y component of turbulent intensity; in fact, on the vertical face of the step $\overline{v^2}$ is more analogous to the x component. The mechanism by which the $\overline{v^2}$ model represents wall effects is described in Ref. 3. Essentially, the $\overline{v^2}$ profile does not have the sharp maximum near the wall that the kinetic energy profiles display upstream of the step in Figs. 5 and 6. Thus, if k is used for the velocity scale, the eddy viscosity is greatly overpredicted near the wall; using $\overline{v^2}$, as in Eq. (8), gives more reasonable values.

Profiles of the dissipation rate are compared to DNS data[11] in Fig. 7. These are at $x = 4, 6, 10,$ and 15 heights downstream of the step, corresponding to locations in Fig. 5; however, here the
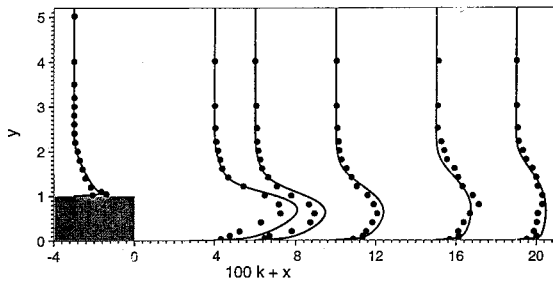
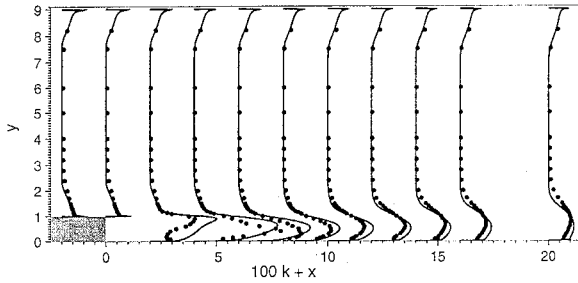**Fig. 5** Turbulent kinetic energy profiles for the Jovic and Driver experiment.

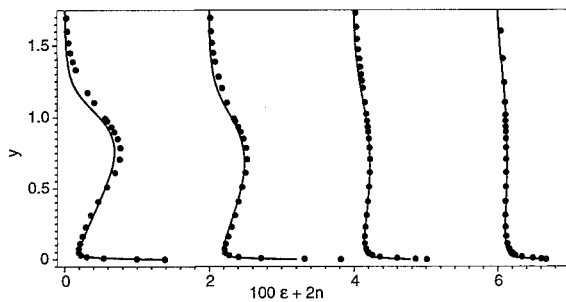**Fig. 6** Turbulent kinetic energy profiles for the Driver and Seegmiller experiment.

Fig. 7 Profiles of dissipation rate with DNS data of Le et al.[11]

Fig. 8 Mean velocity profiles in the Obi et al. diffuser, both Eq. (9) (———) and a constant value of 1.55 (– – –) were used for $C_{\varepsilon_1}^z$, light dashed lines show the diffuser surface.

Fig. 9 Contours of U velocity component in the Obi et al. diffuser: (———) positive values; (– – –) negative values.

Fig. 10 Turbulent kinetic energy profiles in the Obi et al. diffuser.

profiles are displayed with the origin simply shifted by 2 units. This figure illustrates how ε has a sharp peak at the lower wall. This peak emerges naturally when the k-ε system is solved with the no-slip condition on k and no boundary condition on ε. The first and last profiles, at $x = 4$ and 15, are in surprisingly good agreement with the data. At the intermediate positions the magnitude of ε at $y = 0$ is underpredicted. The variable ε plays multiple roles: it is the rate of energy dissipation in Eq. (2); it determines the length scale of nonlocal effects in Eq. (5); it determines the relaxation time scale in Eqs. (2) and (5); and it sets the Lagrangian correlation time scale (which is assumed proportional to the relaxation time scale) in Eq. (8). Figure 7 only speaks to its role as energy dissipation.

Separated Diffuser

Obi et al.[13] measured the flow in a one-sided, 10-deg, plane diffuser. The expansion ratio of 4.7 was sufficient to produce a separation bubble on the sloping wall; hence, this provides a test case for smooth, adverse pressure driven separation. The entrance to the diffuser consisted of a long plane channel (aspect ratio 35) to produce fully developed flow. The Reynolds number based on the half-height of this channel was 10,000. The computational inflow profiles were obtained by solving fully developed channel flow with a parabolic code. In the figures lengths are scaled on the half-height of the inlet channel, and velocities are scaled on its centerline velocity.

Figure 8 shows profiles of $10U + x$. The boundary of the diffuser is indicated in the figure; note, however, that the aspect ratio of this figure is not unity: the actual duct is more elongated, as shown in Fig. 9. Only a portion of the diffuser is shown: the lower wall starts at $x = -6$, $y = 0$ to the left of the figure, and extends to $x = 94$, $y = -7.4$ to the right. The 10-deg, sloping section begins at $x = 0$.
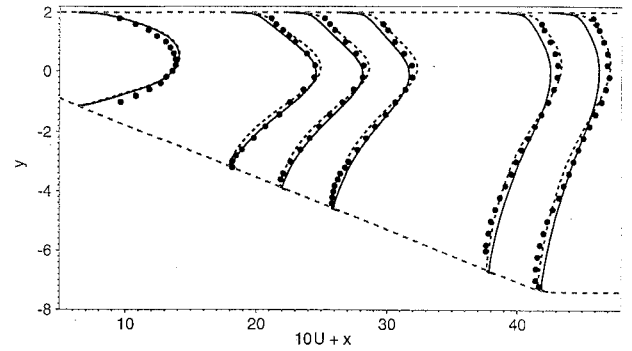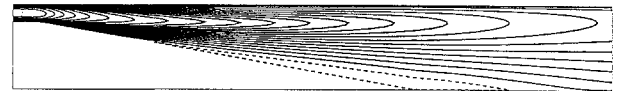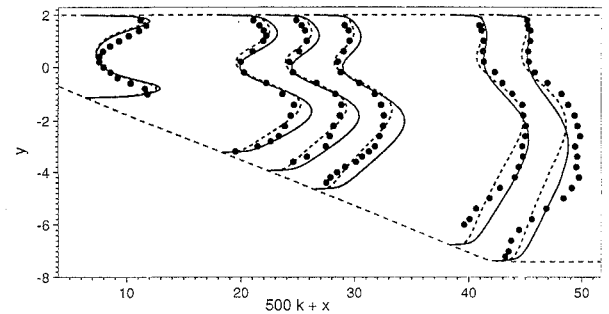
The solid curves in Fig. 8 are a computation using formula (9), whereas the dashed curves show an earlier computation in which the boundary-layer value of $C_{\varepsilon_1}^z = 1.55$ had been used. Expression (9) gives slightly less extensive separation than the constant value $C_{\varepsilon_1}^z = 1.55$. Note that the mass flux is constant, so less backflow near the lower wall is necessarily accompanied by less forward flow in the upper part of the channel. The two cases in this figure illustrate how $C_{\varepsilon_1}^z$ controls the rate of growth of the boundary layer and, hence, the extent of separation. Nevertheless, it is clear that the k-ε-$\overline{v^2}$ formulation is capable of describing the smooth separation.

Figure 9 is a set of constant U contours; the dashed contour corresponds to $U < 0$ and shows the extent of the separated region. This can be compared to the sketch of the separated region in Obi et al.[13] The location and extent of the separated region is very similar to that found in the experiment. Obi et al.[13] computed this flow with the k-ε model and with a second-moment closure, in both cases using wall functions. The k-ε computation showed no separation, whereas the second-moment closure suggested a tiny region of reversed flow, greatly less than measured. The present results are in rather better agreement to the data; if anything, they show slightly too much separation.

Again, the focus in this paper is on mean flow properties; however, turbulent kinetic energy profiles for the Obi et al.[13] experiment are included in Fig. 10. They are plotted as $500k + x$ and computations are shown for the same two cases as in Fig. 8. Toward the outlet of the diffuser the experimental values of k become noticeably larger than the solution to the model, except near the wall. It was remarked in Ref. 11 that three dimensionality became significant farther downstream. This might in part be responsible for the higher fluctuations in the experiment.

Vortex Shedding Behind a Triangular Cylinder

The flow around a triangular cylinder was measured by Twigge–Molecey and Baines[14] and by Sjunnesson in Ref. 15. This geometry
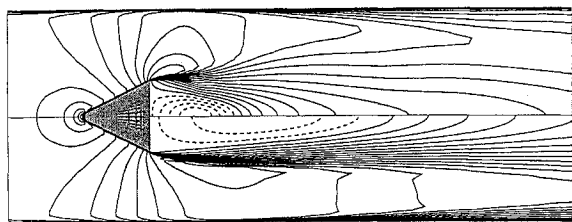
Fig. 11 U contours for a steady calculation (lower-half) and time average of an unsteady computation with vortex shedding (upper-half).
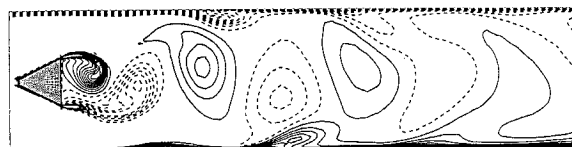

Fig. 12 Instantaneous vorticity contours showing shedding in the time-accurate computation.

provides an example of bluff body flow with fixed separation points. We will compare to the data of Sjunnesson, as presented in Johansson et al.[15] The study by Sjunnesson was motivated by the application to flame holders. The geometry consists of a 6:1 aspect ratio equilateral triangular cylinder centered symmetrically in a duct three cylinder sides high. The Reynolds number based on the cylinder side and inlet velocity was about 42,500. It is known[16] that the Strouhal number of vortex shedding from circular cylinders of this aspect ratio is reduced by about 15% below the infinite aspect ratio value. Indeed, our computations produced a Strouhal number of 0.285, whereas the experimental value was 0.25. The high blockage in this experiment increases the Strouhal number. At a Reynolds number of 4×10^4 Twigge–Molecey and Baines[14] obtained $St = 0.19$ in the absence of blockage. In experiments at a Reynolds number of 1.1×10^4 they found a 15% increase of St for a blockage ratio as low as 0.04.

The data in Figs. 9 and 10 of Johansson et al.[15] were digitized and are shown here in our Figs. 13 and 14. Velocities are normalized by the reported inlet velocity of 17 m/s. Lengths are scaled on the height of the cylinder, which lies between $y = \pm 0.5$.

By taking a large artificial time step, on the order of the shedding period in length, we obtained symmetric, steady solutions to the k-ε-$\overline{v^2}$ model. On introducing an asymmetric disturbance and taking a smaller step, an oscillatory solution was obtained. Figure 11 is a composite showing the time-averaged U contours of the unsteady computation in the upper-half and the steady-state solution in the lower-half. It shows that the steady-state separation bubble is over twice as long as the averaged, unsteady bubble. This figure also illustrates the flow geometry. To generate a grid that efficiently resolves the separating shear layer, the upstream tip of the triangle was flattened. The grid passes through the downstream face and exits the flattened tip, with the part interior to the triangle blanked out. The figure shows the region $-2 < x < 6$; the entire computational domain was $-3 < x < 15$.

Instantaneous vorticity contours, in Fig. 12, show the asymmetric flow in the time-accurate computation. The interaction between the vortex street and the boundary layers in the side walls results in eruption of secondary vorticity. The complexity of such interactions underscores the need to resolve the coherent vortices in this type of flow.

Time-accurate computations, averaged over one period are compared to experimental data in Figs. 13 and 14. Figure 13 shows the U component along the centerline of the cylinder. The centerline velocity of the symmetric, steady solution is also shown. It overpredicts the length of the backflow region by a factor of two. The averaged unsteady solution is in good agreement with the data, although the maximum backflow velocity is a bit lower than the measurements. The unsteady computation is rather more expensive computationally, but it can be seen that unsteady computations are necessary to predict the turbulent flow around a bluff body with coherent vortex shedding.
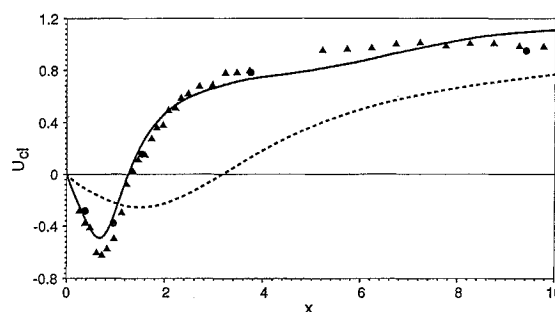

Fig. 13 Time-averaged centerline velocity downstream of triangular cylinder: (——) unsteady computation; (- - -) steady computation; data presented in Ref. 15, Fig. 9 (▲) and Fig. 10 (●).
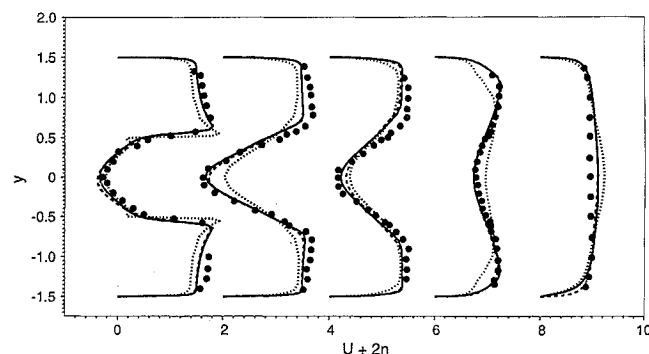

Fig. 14 Time-averaged velocity profiles in the wake of a triangular cylinder: calculations are shown for three grids: 141 × 101 (——), 121 × 91 (- - -); and 71 × 51 (· · · ·)

Figure 14 shows time-averaged velocity profiles in the wake. The profiles are displayed evenly spaced, but the actual locations were $x = 0.375, 0.95, 1.525, 3.75,$ and 9.4 heights downstream of the rear face of the cylinder. The agreement between experiment and model is excellent. The first profile, at $x = 0.375$, shows the sharp boundary and large velocity deficit of the near wake. By $x = 0.95$ the wake profile has altered substantially and is undergoing transition to a Gaussian form.

Computations with 71 × 51, 141 × 101, and 121 × 91 meshes are included in Fig. 14. The grids were nonuniform, having higher resolution in the boundary layers along all surfaces and in the shear layers leaving the trailing edges. The 71 × 51 grid clearly is too coarse to resolve the separated shear layer, but the 141 × 101 grid provides adequate resolution. The 141 × 101 grid was generated with the same algorithm as the 71 × 51 grid by doubling or halving parameters, as appropriate. Unsteady vortex shedding was obtained on the coarse grid, but it is clear that grid refinement is needed to produce a solution of acceptable accuracy.

Reference 15 presents computations of this flow with the k-ε model and wall functions. They show a similar level of agreement with the data to those obtained here. It is fair to surmise that the downstream development of the time-averaged flow is effected largely by deterministic vortex shedding, with the stochastic turbulence playing a secondary role. A corollary is that this flow is not very sensitive to the details of the turbulence model.

Conclusions

It has been shown that the k-ε-$\overline{v^2}$ formulation is viable for computing the mean properties of highly nonequilibrium turbulent flows. The basic mathematical formulation is computationally tractable; indeed, in the test cases, we found robust convergence to steady-state solutions. The equations were solved with no-slip conditions imposed on solid surfaces; no wall, or damping functions were needed. In the previous application of k-ε-$\overline{v^2}$ to boundary layers,[4] the elliptic relaxation equation reduced to an ordinary differential equation. The present computations invoked the full ellipticity of the two-dimensional Laplacian in Eq. (5).

The diffuser and backstep computations showed that the model can be used in flows with smooth separation and with large

separation bubbles. The coefficient $C_{\varepsilon_1}^z$ controls shear layer growth, as in the k-ε model. At present, discrepancies with experiment are as likely due to inaccuracies in the ε equation as to any fault in the $\overline{v^2}$-f_{22} formulation.

The computation of vortex shedding behind a triangular cylinder illustrates the application of k-ε-$\overline{v^2}$ to flows with deterministic unsteadiness. Rodi[17] has described applications of k-ε and Reynolds stress models to vortex shedding. In some cases the k-ε model with wall functions erroneously did not produce vortex shedding. Although this may well be due to inadequate numerical resolution, the possibility exists that in some circumstances it is necessary to integrate to the surface, resolving the viscous wall layer, in order to produce vortex shedding. We did preliminary computations of flow over a square cylinder and flow leaving a thick splitter plate. In both cases a solution with periodic vortex shedding was obtained, provided that the grid resolution within the boundary layer was adequate; under-resolved computations sometimes would not shed, even when subjected to large, asymmetric perturbations.

When deterministic unsteadiness is present, the turbulence is not statistically stationary and time averaging cannot be substituted for ensemble averaging. The turbulence model represents fluctuations relative to the ensemble average, not the time average; the temporal variability of the mean flow must be computed explicitly. It is clear from Figs. 13 and 14 that the k-ε-$\overline{v^2}$ model gives very good predictions for the time-averaged flow when nonstationarity is recognized.

Acknowledgments

References

[1]Rodi, W., and Scheuerer, G., "Scrutinizing the k-ε Model Under Adverse Pressure Gradient Conditions," *Journal of Fluids Engineering*, Vol. 108, 1986, pp. 174–180.

[2]Launder, B. E., "Low Reynolds Number Turbulence Near Walls," UMIST Mechanical Engineering Dept., 1986, Rept. TFD/86/4, Univ. of Manchester, England, UK.

[3]Durbin, P. A., "Near-wall Turbulence Closure Modeling Without 'Damping Functions'," *Theoretical and Computational Fluid Dynamics*, Vol. 3, No. 1, 1991, pp. 1–13.

[4]Durbin, P. A., "Application of a Near-wall Turbulence Model to Boundary Layers and Heat Transfer," *International Journal of Heat and Fluid Flow*, Vol. 14, No. 4, 1993, pp. 316–323.

[5]Coles D. E., and Hirst, E. A., *Computation of Turbulent Boundary Layers*, Air Force Office of Scientific Research, AFOSR-Internal Flow Program-Stanford Conf., Stanford, CA, Aug. 1968.

[6]Rogers, S. E., and Kwak, D., "Upwind Differencing Scheme for the Time-Accurate Incompressible Navier–Stokes Equations," *AIAA Journal*, Vol. 28, No. 2, 1990, pp. 253–262.

[7]Rogers, S. E., Kwak, D., and Kiris, C., "Steady and Unsteady Solutions of the Incompressible Navier–Stokes Equations, *AIAA Journal*, Vol. 29, No. 4, 1991, pp. 603–610.

[8]Ko, S., "Computation of Turbulent Flow over Backward and Forward-facing Steps Using a Near-wall Reynolds Stress Model," Center for Turbulence Research, Stanford Univ., *Annual Research Briefs*, 1993, pp. 75–90.

[9]Jovic, S., and Driver, D., "Backward-facing Step Measurements at Low Reynolds Number," NASA TM 108807, 1994.

[10]Driver, D., and Seegmiller, H. L., "Features of a Reattaching Turbulent Shear Layer in Divergent Channel flow," *AIAA Journal*, Vol. 23, No. 2, 1985, pp. 163–171.

[11]Le, H., Moin, P., and Kim, J., "Direct Numerical Simulation of Turbulent Flow over a Backward-facing Step," Thermosciences Div., Dept. of Mechanical Engineering, Rept. TF-58, Stanford Univ., 1993.

[12]Rodi, W., "Experience with Two-Layer Models Combining the k-ε model with a One-Equation Model near the Wall," AIAA Paper 91-0216, 1991.

[13]Obi, S., Ohimuzi, H., Aoki, K., and Masuda, S., "Experimental and Computational Study of Turbulent Separating Flow in an Asymmetric Plane Diffuser," *9th Symposium on Turbulent Shear Flows*, Kyoto, Japan, Aug. 1993, pp. P305-1–P305-4.

[14]Twigge-Molecey, C. F. M., and Baines, W. D., "Aerodynamic Forces on a Triangular Cylinder," *Journal of Engineering Mechanics*, Vol. 99, Aug. 1973, pp. 803–818.

[15]Johansson, S., Davidson, L., and Olsson, E., "Numerical Simulation of the Vortex Shedding past Triangular Cylinders at High Reynolds Number Using a k-ε Turbulence Model," *International Journal of Numerical Methods in Fluids*, Vol. 16, No. 6, 1993, pp. 859–878.

[16]Gerich, D., and Eckelmann, H., "Influence of End Plates and Free Ends on Shedding Frequency of Circular Cylinders," *Journal of Fluid Mechanics*, Vol. 122, Sept. 1982, pp. 109–122.

[17]Rodi, W., "On the Simulation of Turbulent Flow past Bluff Bodies," *Proceedings of the 1st International Symposium on Computational Wind Engineering*, Tokyo, 1992, pp. 3–19.